Supplemental Information: Accuracy and precision of near-field HEDM forward-model based microstructure reconstructions

D.B. Menasche,[a*1] P.A. Shade[b] and R.M. Suter[a]

[a] *Physics Department, Carnegie Mellon University, 5000 Forbes Ave., Pittsburgh, PA, 15213, USA, and* [b] *Materials and Manufacturing Directorate, Air Force Research Laboratory, Wright-Patterson AFB, OH 45433, USA.*

E-mail: david.menasche@hamiltoniangroup.com

1. Supplemental Information

1.1. Determination of affine transformation to correct EBSD grain map

To accomplish determination of the discussed transformation, the edges of Fig. 2(b) were segmented by thresholding the pixel intensity value at half of the average maximum intensity characteristic to the sample material. Due to the high dynamic range of the image and the large intensity contrast between material and air, the rise width at the sample edge was very small, $\sim$ 100 nm, so errors associated with this thresholding are negligible when compared to the nf-HEDM spatial errors. To extract the edges from the EBSD grain map, first a threshold was applied on TSL's 'quality' parameter. The quality is taken to be a figure of merit for each reconstructed voxel of the EBSD scan. Edges were then found by identifying EBSD voxels with fewer than four nearest neighbors on the square grid. These EBSD map edges were aligned to the

[1] Now of Hamiltonian Group LLC.

edges segmented from Fig. 2(b) using an affine optimization procedure described later. In practice, arbitrariness associated with choosing the $\mathcal{Q}$ threshold was removed by assigning Fig. 2(b) as the ground truth for Fig. 2(a). Values for $\mathcal{Q}$ were chosen in the range $[0, 1]$, while iteratively performing affine optimization. The threshold that gave the best correspondence between boundary sets after affine optimization was selected. Ultimately $\mathcal{Q} = 0.35$ resulted in the most optimized match.

Before affine optimization, a manual inversion across the y-axis was applied to harmonize the coordinate axes of the two images. Subsequently, seeded Monte Carlo was employed to optimize the registration of the specimen edges. A transformation, A, of the form

$$A = \begin{pmatrix} \cos(\phi) + \delta_{11} & -\sin(\phi) + \delta_{12} & \Delta x + \delta_{13} \\ \sin(\phi) + \delta_{21} & \cos(\phi) + \delta_{22} & \Delta y + \delta_{23} \\ 0 & 0 & 1 \end{pmatrix} \tag{1}$$

was applied to the segmented edge points from the EBSD map. Guesses for ϕ, Δx, and Δy were obtained by hand, after which six-tuples of $\{\delta_{11}, \delta_{12}, \delta_{13}, \delta_{21}, \delta_{22}, \delta_{23}\}$ were generated, each defining a transformation. A cost was defined for each of these transformations,

$$\mathcal{C} = \frac{1}{N_{\mathrm{S}}} \sum_{i=1}^{N_{\mathrm{S}}} \min_{j=1}^{N_{\mathrm{E}}} \left| \vec{r}_{i,\mathrm{S}} - \vec{r}_{j,\mathrm{E}} \right| \tag{2}$$

where N_{S} is the total number of edge points segmented from Fig. 2(b), N_{E} is the total number edge points segmented from the indexed EBSD map, $\vec{r}_{i,\mathrm{S}}$ are the edge points segmented from the SEM data set, and $\vec{r}_{j,\mathrm{E}}$ are the sample edge points segmented from the EBSD map, transformed by a particular transformation. This form was chosen for $\mathcal{C}$ to inform the error in this registration; here $\mathcal{C}$ is the average minimum distance from an edge point in the SEM data set to the corresponding edge point in the EBSD data set.

1.2. Justification that finite beam height effects are negligible

While finite beam height effects can play a role in spatially resolved orientation (and thus grain boundary) determination, we find that for all grain boundaries this effect is small and does not affect the conclusions above. The nf-HEDM reconstruction process assumes a perfectly planar beam, but for this experiment, the florescence measurement determined its height to be 1.8 μm. Fig. S1 shows a one-dimensional example of how, when measuring a surface, this finite beam height can introduce errors that depend on ϕ, the angle between grain boundary normal and the surface plane. The error in this case is easily determined to be $\delta r = \delta z \tan(\phi)$, with $\delta z = 0.9$ μm, half the beam FWHM. This establishes 0.90 μm as the upper bound for errors due to this effect, fully realized only for grains with 45° inclination. The situation is made slightly more complicated for the case in which the sample is tilted with respect to the beam.

Fig. S2 shows a one-dimensional example of this case. We define $r = 0$ to be the location where the brightest part of the beam profile intersects the sample surface. We define r to be the distance between the intersection of the grain boundary with the brightest part of the beam profile and $r = 0$, and ψ is the angle between the sample surface and the beam. The first assumption required to treat this effect is that the microstructure reconstructed will be the region illuminated by the brightest part of the Gaussian beam that intersects that cross section. The justification for this is that the signal will be stronger for the diffraction originating from that part of the cross section. For an incoming beam intersecting a bulk sample, the cross section reconstructed will be that which intersects the peak of the Gaussian beam profile.

As always, only that volume which is illuminated can diffract. If only the tail of the beam intersects the sample surface, the brightest part of the beam will result in the dominating signal, and in that case, the volume nearest the sample surface gives the most signal. The origin of the strongest signal (thus the cross section reconstructed) is

highlighted in yellow dashed in Fig. S2. By these arguments, only regions where $r > 0$ require correction. In this figure, δr is the error in the assumed surface boundary position from being a height δz below the surface point relative to the planar cross section. Assuming that ψ can be estimated, then δz can be found for a given point on the reconstruction by

$$\tan\psi = \frac{\delta z}{r + \delta r}. \tag{3}$$

Given a grain boundary inclination (relative to the reconstruction) of ϕ, then

$$\tan\phi = \frac{\delta r}{\delta z} \tag{4}$$

or

$$\delta r = \frac{r\tan\psi\tan\phi}{1 - \tan\psi\tan\phi}, \tag{5}$$

using Eq. 3. By inspection of Fig. 3, the normal to the tilt plane of the sample with respect to the beam lays almost completely in the yz plane, thus requiring correction of the boundary locations along $\hat{y}$ only, as an initial approximation. Unfortunately, it is not possible to set the origin of $\hat{r}$, *i.e.* the location where the peak of the Gaussian beam intersects a cross section. We know the point where the tail of the beam intersects z_0 because diffracted signal stops being reconstructable where there is material, at about the start of the trench feature. We do not know how far this cross section would extend, however, because of the absence of material to reconstruct beyond grain #8. We do know a sure upper bound for ψ, by assuming the cross section of z_0 spans only grain #8 to the point where the reconstruction stops, a total of 91 μm along $\hat{y}$. The beam is 1.8 μm at the FWHM, so $\psi_{\max} \leq \tan^{-1}(1.8/91) = 1.13°$. In reality, this is probably an over-estimate; there is no clipping of grain #8 at the top of z_0 in Fig. 3, and C is comparatively low at the bottom of the reconstruction, evidence that the tail of the beam illuminated that section of microstructure. We see no corresponding drop at the top of the structure, save for the grain #8 which has reduced C values in each

cross section. This implies perhaps that better initial alignment may have illuminated the entire surface volume, tilt or not, within the $\sim 2\ \mu$m beam height. Regardless of our inability to set the origin for r, by examining ϕ for each grain boundary, we can achieve some estimate of the magnitude of these finite beam-height errors.

Extracting grain boundary traces for each cross section and performing principal component analysis on each group of boundary points gives a grain boundary normal and a measure for ϕ along $\hat{y}$ for the grains extracted. These boundary traces are plotted in Fig. S3 and are colored by the measured ϕ value. They are depicted in the original reference frame of the reconstructions, *i.e.* that of Fig. 3. The points plotted include boundary segments from the first four cross sections. With a boundary-averaged ϕ value computed for each grain boundary, plausible values for δr may be calculated by examining possible values for r and ψ. This is done for each of the boundaries enumerated in Fig. S3 for $r \in [10, 40]\ \mu$m and $\psi \in [0.5^\circ, 1.1^\circ]$, with the results plotted in Fig. S4. Within these ranges, errors from the finite-beam-height approximation are less than 0.3 μm for all non-twin boundaries and less than 0.5 μm for the twin boundaries. From this we confirm that the planar beam approximation does not affect our previous conclusion that on average the orientation determination is spatially accurate to the limit set by the resolution of CCD detector used.

2. Supplemental Figures

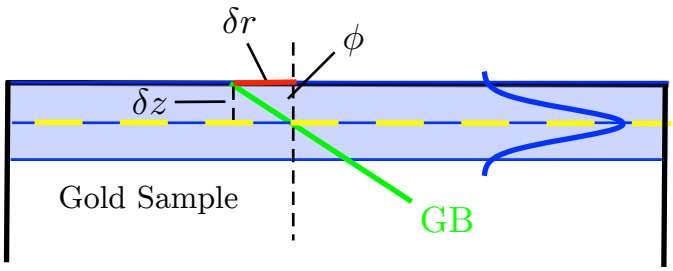

Fig. S1. A one dimensional example of the error, δr, of interpreting the reconstructed microstructure as the surface microstructure if the bulk of the diffracted signal occurs below the surface. This assumes no tilt of the sample with respect to the beam. The reconstructed cross section appears dashed. A grain boundary is depicted in green; the angle between the grain boundary and the normal to the sample surface is ϕ. Here, the Gaussian beam profile is depicted in blue, with the illuminated area also in blue.

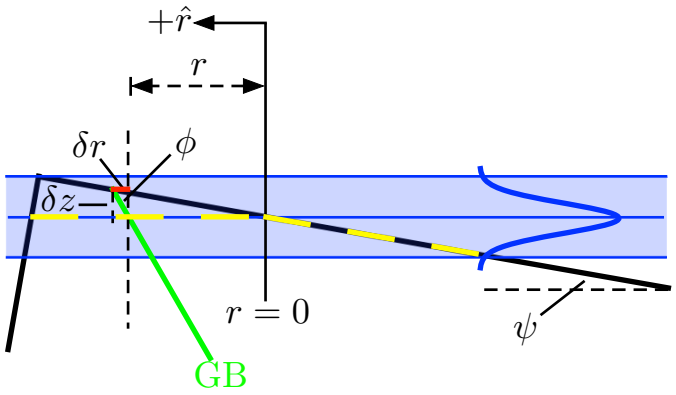

Fig. S2. The error, δr, of interpreting the reconstructed microstructure as the surface microstructure if the bulk of the diffracted signal occurs below the surface, given additional tilt between the sample surface and the beam. The reconstructed cross section appears dashed. We define $r = 0$ to be the intersection between the maximum of the beam profile and the surface of the sample. We define distance r to be the distance between $r = 0$ and the intersection of the grain boundary with the maximum of the beam profile. δr depends both on the tilt of the specimen *vis-a-vis* the beam, ψ, and the measured grain boundary inclination angle, ϕ. Here, the Gaussian beam profile is depicted in blue, with the illuminated area also in blue. See text for a full description.

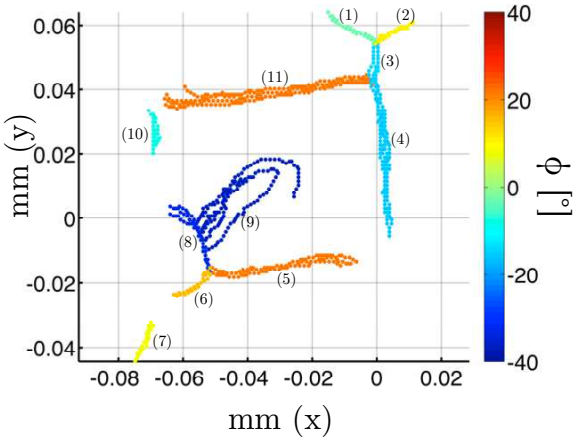

Fig. S3. The grain boundary traces extracted, colored by ϕ, their grain boundary inclination angles relative to $\hat{y}$. Most boundaries have an inclination less than 20°, implying very small errors due to finite beam height. Boundaries (8) and (9) deviate most strongly from this trend and show the most discrepancy in measured boundary position.

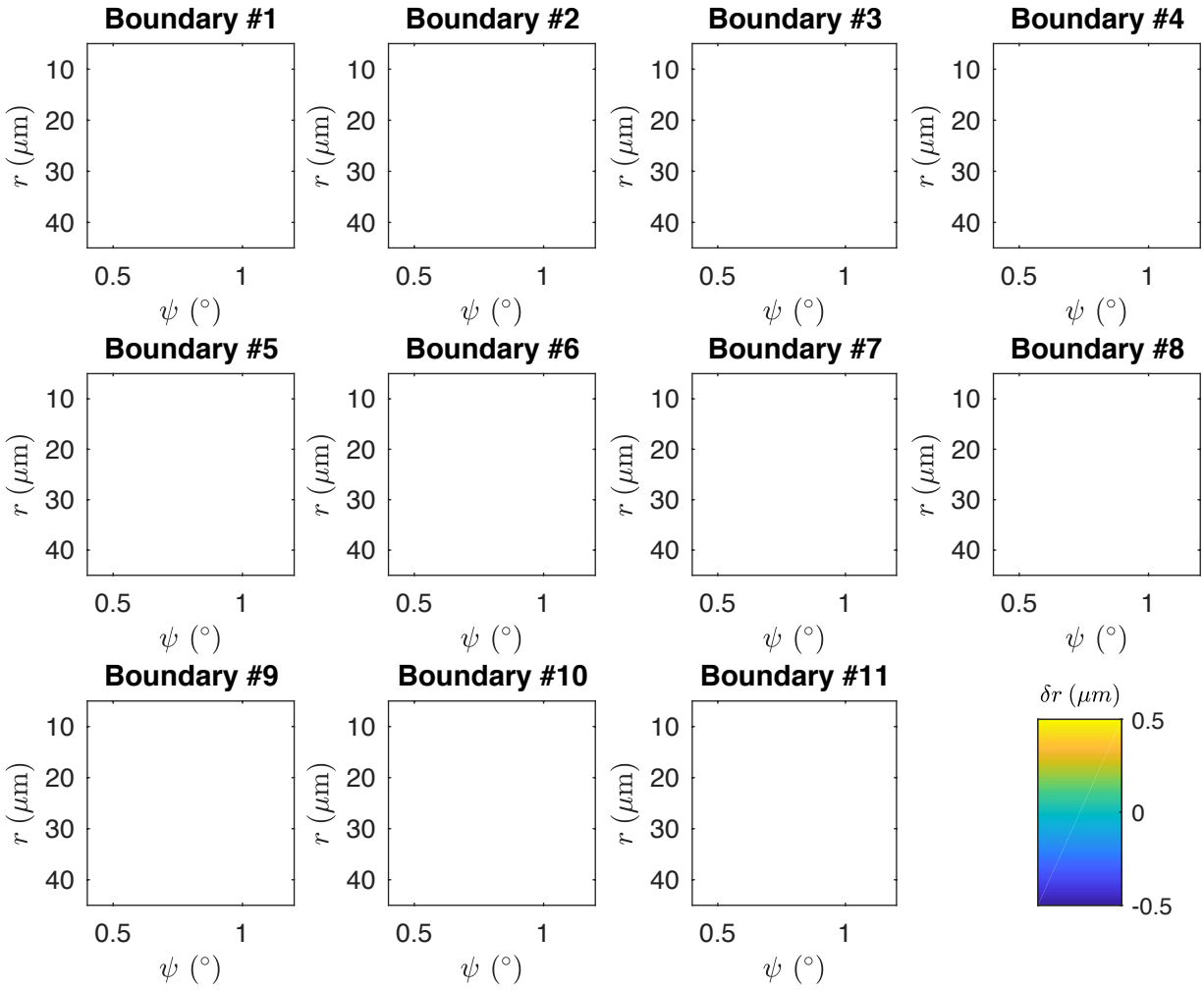

Fig. S4. Panel illustrating the susceptibility of each grain boundary to localization errors associated with finite beam height. r is the distance between the grain boundary's intersection with the maximum of the beam profile and the intersection of the maximum of the beam profile with the surface of the sample. ψ is the angle between the sample surface and the beam. Each panel is colored by the magnitude of the error, δr. Because neither r nor ψ can be precisely determined, we show the values of δr for a conservative range of values.